Point sink flow in a linearly stratified fluid of finite depth

Kataoka, Takeshi

Tsutahara, Michihisa

Tanaka, Masaya

(Citation)
Physics of Fluids,12(11):2775-2786

(Issue Date)
2000-11

(Resource Type)
journal article

(Version)
Version of Record

(URL)
https://hdl.handle.net/20.500.14094/90001172

Point sink flow in a linearly stratified fluid of finite depth

Takeshi Kataoka,[a] Michihisa Tsutahara, and Masaya Tanaka
Graduate School of Science and Technology, Kobe University, Rokkodai, Nada, Kobe 657-8501, Japan

(Received 15 July 1999; accepted 26 July 2000)

The evolution of selective withdrawal through a point sink of horizontally unbounded, linearly stratified fluid of finite depth is studied as an initial-value problem. Following the initiation of discharge from the sink, internal gravity wave modes propagate radially upstream to change the flow pattern. These modes are called cylindrical modes. We first consider the case of $F \to 0$ (where F is the Froude number) to get linearized governing equations, and seek a linear asymptotic solution for large times t^* after starting the discharge, of the cylindrical modes in a stratified fluid where viscous and diffusive effects are negligible. The obtained solution shows that the strength of the modal front grows like $t^{*1/3}$, unlike the case of two-dimensional modes whose strength at the front is kept constant. Numerical calculations are also performed to study the case of $F > 0$. The results then indicate that all the cylindrical modes can propagate upstream for any F except infinity. The steady-state withdrawal-layer thickness and time to steady state are also investigated over the full parameter range considering the viscous and diffusive effects. The obtained results are then compared with both the analytical and experimental results of prior works. © *2000 American Institute of Physics.* [S1070-6631(00)00611-5]

I. INTRODUCTION

There are various interesting phenomena that happen in stratified fluids where the density varies in the vertical direction. For example, when fluid is withdrawn from a sink situated in a density-stratified reservoir, only a layer of fluid adjacent to the sink level is withdrawn. This phenomenon, called selective withdrawal, has wide application in engineering aspects, such as withdrawal of cooling water for power plants and water quality management in reservoirs.[1] Therefore many researchers have studied it using two-dimensional flow, or line sink flow of linearly stratified fluid as its simple model.

The study of this problem was initiated by Yih,[2] who obtained the steady-state theoretical solution of selective withdrawal through a line sink of an inviscid stratified fluid of finite depth. His solution showed the uniform withdrawal of fluid from all depths when the Froude number $F_2 = q/Nd^2$ is larger than the critical Froude number $F_{2c} = 1/\pi$, where q is the discharge per unit length of the line sink located at the middepth of the fluid, N is the buoyancy frequency, and $2d$ is the depth of the fluid. His solution, however, showed breakdown when $F_2 < F_{2c}$ due to inadequacy of the uniform flow boundary condition far upstream, which means that the selective withdrawal occurs for $F_2 < F_{2c}$. This fact was verified by experiments conducted later by Debler.[3] Pao and Kao[4] were the first to clarify the time-dependent evolution of the selective withdrawal. They showed by linearized theory (which corresponds to an assumption that $F_2 \to 0$) that the successive propagation of so-called columnar disturbance modes are responsible for the development of flow concentration. Various features of the line sink flow, such as propagation of two-dimensional modes,[4–8] evolution of selective withdrawal,[4–7,9] steady-state flow patterns,[2–5,7,9–13] etc., have been investigated enormously and elucidated so far.

In contrast, comparatively few works have been done on axisymmetric withdrawal or a point sink flow[14–18] that seems to be of more practical interest than the line sink flow. The geometry of the point sink flow is shown in Fig. 1. In this case a series of cylindrical modes travels out from the sink and the flow is characterized by the three parameters: the Froude number F, the Grashof number Gr, and the Schmidt number Sc, defined by

$$F = Q/Nd^3, \quad \mathrm{Gr} = N^2 d^4/\nu^2, \quad \mathrm{Sc} = \nu/D, \tag{1}$$

where Q is the discharge from the point sink, ν is the kinematic viscosity, and D is the diffusivity of stratifying species.

Yih[14] treated the point sink flow of an inviscid, nondiffuse stratified fluid ($\mathrm{Gr} \to \infty$ and $\mathrm{Gr}^{1/2}\mathrm{Sc} \to \infty$) of finite depth as a steady-state problem to show that, if F is finite, no steady-state solution can satisfy a boundary condition of potential flow far upstream. In contrast, Lawrence[15] treated this inviscid flow as a time-dependent problem. He showed by linearized theory (which corresponds to an assumption that $F \to 0$) that linear cylindrical modes propagate horizontally upstream at the same speed as that of the two-dimensional modes. He, however, resorted to the hydrostatic approximation to simplify the solution in which no waves of short horizontal wavelength are described. His solution is also singular at the modal front.

Steady-state withdrawal-layer thickness was first investigated by Koh,[16] who showed by linearized theory ($F \to 0$) that it is proportional to $(\mathrm{Gr\,Sc})^{-1/6} r^{*1/3} d^{2/3}$ (r^* is a radial distance from the sink) in the flow regime where viscous

[a]Author to whom all correspondence should be addressed; electronic mail: kataoka@mech.kobe-u.ac.jp

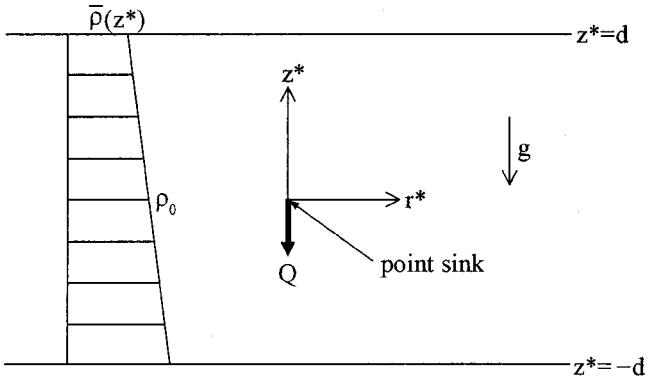

FIG. 1. Geometry of the point sink flow.

forces and species diffusion are dominant. Lawrence[15] and Spiegel and Farrant[17] carried out their experiments to find that, in the inertial regime where inertia and buoyancy forces are important, the withdrawal-layer thickness is independent of distance from the sink and of order $F^{1/3}$. Later Ivey and Blake[18] applied scaling analysis introduced by Imberger *et al.*[9] to the point sink flow problem and classified it into the three basic types of steady-state flow regimes: (i) inertial-buoyancy regime, (ii) viscous-convective regime, (iii) viscous-diffusive regime. The range of the parameters for each regime, the corresponding steady-state withdrawal-layer thickness, and time to steady state are summarized in Sec. V B of the present paper. It was found that Koh's analytical result[16] falls on regime (iii) and the experimental results of both Lawrence[15] and Spiegel and Farrant[17] fall on regime (i). Ivey and Blake[18] themselves also conducted their experiments for regimes (i) and (ii). No experiments, however, have been made for regime (iii). It also should be noted that experiments of the point sink flow are attended with difficulty in measuring the flow velocity, and also with the effects of endwall whose influence on the flow is different from experiments to experiment depending on, for example, the size of containers. Therefore theoretical or numerical study is required to clarify the fundamental nature of sink-initiated motion of stratified fluid.

In this paper, we consider an initial-value problem of the point sink flow in an infinite-horizontal-extent fluid (see Fig. 1). We follow prior studies[2,4,6,7,9–15,18] by considering the case of finite-depth fluid between two horizontal free-slip planes in order to avoid complexities caused by the surface gravity waves or the boundary-layer effects and obtain a fundamental understanding of the point sink flow in a stratified fluid. We first investigate the behavior of linear cylindrical modes in a stratified fluid where viscous and diffusive effects are negligible ($F\to 0$, $\mathrm{Gr}\to\infty$, and $\mathrm{Gr}^{1/2}\,\mathrm{Sc}\to\infty$ where the withdrawal-layer thickness approaches zero throughout the entire flow field as time increases) analytically, and make a comparison with that of the two-dimensional modes. We use the stationary phase method to obtain an asymptotic behavior of these modes for large times after starting the discharge. The obtained solution is subject to no wavelength approximation, unlike previous works, so that it describes the modal front and all wave components properly. Next, numerical calculations are made to clarify the behavior of these cylindrical modes for arbitrary parameters. We are especially interested in the dependence of their behavior on the parameter $F(>0)$. We also investigate the steady-state withdrawal-layer thickness and time to steady state for the three regimes suggested by Ivey and Blake.[18] The results are then compared with both the analytical and experimental results of prior works.

In Sec. II, we shall formulate the equations of motion to show that parameters characterizing the problem are F, Gr, and Sc. In Sec. III, we consider the case of $F\to 0$, $\mathrm{Gr}\to\infty$, and $\mathrm{Gr}^{1/2}\,\mathrm{Sc}\to\infty$ to analytically study the behavior of the linear cylindrical modes. Section IV states the numerical method. In Sec. V, numerical results are presented for flows of $F>0$ to investigate both the nonlinear effects on the mode propagation in an inviscid fluid (Sec. V A) and the withdrawal-layer thickness over the entire parameter range (Sec. V B). Finally, in Sec. VI, concluding remarks are given.

II. FORMULATION

Consider a flow induced by an impulsively started point sink of stratified fluid in a space between two horizontal free-slip planes located at $z^*=\pm d$ ($0<r^*<\infty$, $0<\theta^*<2\pi$, $-d<z^*<d$; $r^*-\theta^*-z^*$ is a cylindrical coordinate system) in which the point sink is located at $(r^*,z^*)=(0,0)$ and the gravitational force g acts in the negative z^* direction. The problem geometry is sketched in Fig. 1. Initially, the fluid is quiescent and linearly stratified in the vertical z^* direction so that the initial density distribution is given by

$$\bar{\rho}(z^*)=\rho_0(1-\kappa z^*), \tag{2}$$

where ρ_0 is the density at $z^*=0$ and κ is a positive constant. Here we are interested in the flow after starting the discharge Q from the point sink at time $t^*=0$. This flow has no θ^* dependence, and hence, is axisymmetric about the z^* axis. The Boussinesq approximation is applied considering the fluid satisfying $\kappa d\ll 1$, which is often the case of most practical situations. The flow is then symmetric with respect to the r^* and z^* axes. Therefore, we analyze this problem only in the first quadrant of an r^*-z^* plane by imposing the free-slip condition on the r^* and z^* axes in the fluid.

We express the time-dependent density distribution $\tilde{\rho}$ as

$$\tilde{\rho}(r^*,z^*,t^*)=\bar{\rho}(z^*)+\rho'(r^*,z^*,t^*), \tag{3}$$

where ρ' is the density fluctuation from its initial value $\bar{\rho}$. We define (u^*,w^*) as the velocity components in the (r^*,z^*) directions and introduce the following dimensionless variables:

$$\begin{aligned}(u,w)&=\left(\frac{u^*}{U_0},\frac{w^*}{U_0}\right),\quad t=Nt^*,\\ (r,z)&=\left(\frac{r^*}{d},\frac{z^*}{d}\right),\quad \rho=\frac{g}{\rho_0 N U_0}\rho',\end{aligned} \tag{4}$$

where $U_0=Q/4\pi d^2$ and $N=(\kappa g)^{1/2}$ are the characteristic velocity and the constant buoyancy frequency, respectively.

Thus, under the Boussinesq approximation, the dimensionless governing equations incorporating the viscous and diffusive effects are given by

$$\frac{\partial \zeta}{\partial t}+\frac{F}{4\pi r}\left[J(\zeta,\psi)-\frac{\zeta}{r}\frac{\partial \psi}{\partial z}\right]=\frac{\partial \rho}{\partial r}+\frac{1}{\mathrm{Gr}^{1/2}}\left(\Delta\zeta-\frac{\zeta}{r^2}\right), \tag{5}$$

$$\frac{\partial \rho}{\partial t}+\frac{F}{4\pi r}J(\rho,\psi)=-\frac{1}{r}\frac{\partial \psi}{\partial r}+\frac{1}{\mathrm{Sc}\,\mathrm{Gr}^{1/2}}\Delta\rho, \tag{6}$$

$$\zeta=\frac{1}{r}\left(\frac{\partial^2\psi}{\partial r^2}-\frac{1}{r}\frac{\partial \psi}{\partial r}+\frac{\partial^2\psi}{\partial z^2}\right), \tag{7}$$

where

$$J(a,b)=\frac{\partial a}{\partial r}\frac{\partial b}{\partial z}-\frac{\partial a}{\partial z}\frac{\partial b}{\partial r},$$

$$\Delta=\frac{\partial^2}{\partial r^2}+\frac{1}{r}\frac{\partial}{\partial r}+\frac{\partial^2}{\partial z^2},$$

and ψ is the stream function satisfying $u=r^{-1}\partial\psi/\partial z$ and $w=-r^{-1}\partial\psi/\partial r$. Note that F, Gr, and Sc are defined by (1). Equation (5) is the so-called vorticity equation where ζ is the dimensionless vorticity [see (7)]. This equation is derived by cross-differentiating the Navier–Stokes equations of motion in the r and z directions. Equation (6) is derived from the equation for the stratifying species by assuming the linear relationship between the concentration of the species and density.[16] Equations (5)–(7) are to be solved under the boundary conditions

$$\begin{aligned}&\psi=0,\quad \zeta=0,\quad \rho=0\quad (r\geqslant 0,\ z=0),\\ &\psi=-1,\quad \zeta=0,\quad \rho=0\quad (r\geqslant 0,\ z=1),\\ &\psi=-1,\quad \zeta=0,\quad \frac{\partial\rho}{\partial r}=0\quad (r=0,\ 0<z<1),\\ &|\psi|<\infty\quad (r=\infty,\ 0<z<1),\end{aligned} \tag{8}$$

and the initial conditions

$$\zeta=0,\quad \rho=0\quad (r>0,\ 0<z<1). \tag{9}$$

Now it is clear that the system (5)–(9) is characterized by the three parameters: F, Gr, and Sc.

III. LINEAR SOLUTION

Substituting $F\to 0$ and $\mathrm{Gr}\to\infty$ (with $\mathrm{Gr}^{1/2}\,\mathrm{Sc}\to\infty$) into (5)–(9), we obtain the following linearized equation in terms of ψ governing the small amplitude motion associated with the point sink flow of a stratified fluid where viscosity and diffusivity are negligible:

$$\frac{\partial^2}{\partial t^2}\left(\frac{\partial^2\psi}{\partial r^2}-\frac{1}{r}\frac{\partial\psi}{\partial r}+\frac{\partial^2\psi}{\partial z^2}\right)+\frac{\partial^2\psi}{\partial r^2}-\frac{1}{r}\frac{\partial\psi}{\partial r}=0. \tag{10}$$

Equation (10) is solved subject to the boundary conditions (8) for ψ and the initial conditions $\zeta=0$ and $\partial\zeta/\partial t=0$.

We now apply the technique of separation of variables, and the solution ψ can be cast into the following form:

$$\psi=-z+\sum_{n=1}^{\infty}\psi_n(r,t)\sin n\pi z. \tag{11}$$

Here ψ_n is a function of r and t satisfying

$$\frac{\partial^2}{\partial t^2}\left(\frac{\partial^2\psi_n}{\partial r^2}-\frac{1}{r}\frac{\partial\psi_n}{\partial r}-n^2\pi^2\psi_n\right)+\frac{\partial^2\psi_n}{\partial r^2}-\frac{1}{r}\frac{\partial\psi_n}{\partial r}=0, \tag{12}$$

with the boundary conditions

$$\psi_n(0,t)=\psi_0,\quad |\psi_n(\infty,t)|<\infty, \tag{13}$$

and the initial conditions

$$\psi_n(r,0)=\psi_0 n\pi r K_1(n\pi r),\quad \frac{\partial\psi_n}{\partial t}(r,0)=0, \tag{14}$$

where

$$\psi_0=-\frac{2}{n\pi}, \tag{15}$$

and K_1 is the first-order modified Bessel function of the second kind. Note that the initial conditions (14) are given by solving $\zeta=0$ and $\partial\zeta/\partial t=0$ in terms of ψ_n under the boundary conditions (13). The second term on the right-hand side of (11) represents a contribution from the vertical modes $\sin n\pi z$ $(n=1,2,...)$ where n is the modal number. The purpose of the present section is to solve the system (12)–(14) to obtain an asymptotic solution of ψ_n for large t with $r/t\sim 1$ that properly describes the propagation of all wave components.

To obtain such an asymptotic solution of ψ_n, it should be expressed in the form of an integral (see Bender and Orszag[19]). So we introduce the Hankel transform in r and the Laplace transform in t, and set

$$\hat{\psi}_n(k,s)=\int_0^\infty \exp(-st)dt\int_0^\infty \psi_n(r,t)J_1(kr)dr,$$

$$\psi_n(r,t)=\frac{r}{2\pi i}\int_0^\infty kJ_1(kr)dk\int_{\gamma-i\infty}^{\gamma+i\infty}\hat{\psi}_n(k,s)\exp(st)ds,$$

where J_1 is the first-order Bessel function of the first kind and γ is a real value that places the path of integration to the right of all singularities of the integrand in the complex s plane. Applying these to (12) and using (13), (14), and $\psi_n(\infty,t)=0$ obtained by evaluating (12)–(14) at $r=\infty$, we get, after some calculation,

$$\psi_n(r,t)=\psi_0 I(n\pi r,t), \tag{16}$$

where

$$I(n\pi r,t)=\frac{r}{2\pi i}\int_0^\infty\frac{k^2J_1(kr)}{k^2+n^2\pi^2}dk \times\int_{\gamma-i\infty}^{\gamma+i\infty}\frac{(s^2+1)\exp(st)}{s[s-i\omega_0(k)][s+i\omega_0(k)]}ds, \tag{17}$$

and

$$\omega_0(k)=\frac{k}{(k^2+n^2\pi^2)^{1/2}}. \tag{18}$$

Carrying out the integration with respect to s, and substituting the following integral representation[20] of J_1,

$$J_1(kr)=\frac{1}{\pi kr}\int_0^\infty p^{1/2}\exp(-p)\times\left\{(2kr+ip)^{1/2}\exp\left[i\left(kr-\frac{3}{4}\pi\right)\right]+(2kr-ip)^{1/2}\exp\left[-i\left(kr-\frac{3}{4}\pi\right)\right]\right\}dp, \quad (19)$$

for the later convenience in making an asymptotic expansion, we obtain

$$I(n\pi r,t)=1-\int_0^\infty p^{1/2}\exp(-p)[I_+(n\pi r,t)+I_-(n\pi r,t)]dp, \quad (20)$$

where

$$I_\pm(n\pi r,t)=\int_{-\infty}^{\infty}(2kr\pm ip)^{1/2}f(k)\exp[i\chi_\pm(k)t]dk, \quad (21)$$

and

$$f(k)=\frac{n^2\pi}{2k(k^2+n^2\pi^2)}, \quad (22)$$

$$\chi_\pm(k)=\omega_0(k)\pm\frac{kr-3\pi/4}{t}. \quad (23)$$

Here the branch cuts emanating from the branch points $k=-ip/2r$ and $ip/2r$ are taken as extending vertically downward and upward, respectively, and the phase of complex square roots of the form $(2kr\pm ip)^{1/2}$ is set to be zero as $k\to\infty$. We also note that the paths of integration must be taken to the same side of the real axis around a simple pole $k=0$ [see (22)] for both I_+ and I_-.

Now we follow Lighthill[21] (see also Bender and Orszag[19]) to carry out an asymptotic expansion of the integral representation $I_\pm$ presented in (21) using the stationary phase method. The stationary points of the integrand of $I_\pm$ are given by

$$\chi'_\pm(k)\equiv\frac{d\chi_\pm}{dk}=\frac{n^2\pi^2}{(k^2+n^2\pi^2)^{3/2}}\pm\frac{r}{t}=0, \quad (24)$$

which yields no real stationary points for the phase χ_+. For the phase χ_-, (24) gives

$$k=\pm k_0\equiv\pm n\pi\left\{\left(\frac{t}{n\pi r}\right)^{2/3}-1\right\}^{1/2}\quad\text{when}\quad\frac{n\pi r}{t}<1, \quad (25)$$

and no real stationary points when $n\pi r/t>1$.

Here we choose paths of integration passing to the left-hand side of the simple pole $k=0$. This choice makes I_+ exponentially small as $t\to\infty$ because the integration path is raised everywhere so as to give the imaginary part of χ_+ a small positive value. But I_- has contribution from this pole when $n\pi r/t>1$ because the path must be lowered everywhere to make the imaginary part of χ_- positive. Only in the vicinity of $k=0$ is the path raised to go round the simple pole in a clockwise sense so that we find from the residue theorem

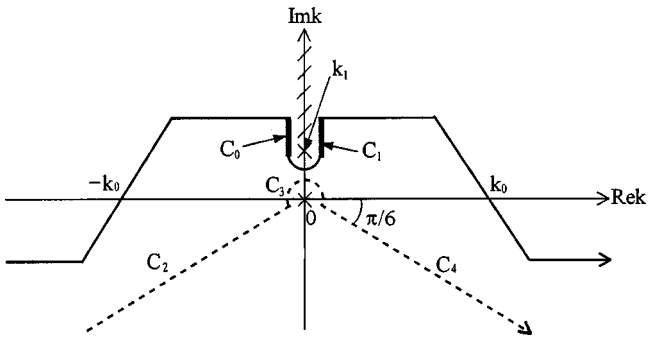

FIG. 2. Branch cut for the integrand of I_-, and deformed paths of integration for the integral I_- when $n\pi r/t<1$ (solid line) and $n\pi r/t\approx 1$ (dashed line). Each path named C_i $(i=0,1,...,4)$ is defined as follows: C_0 (left broad solid line) is given by $k-k_1=se^{-3\pi i/2}$ $(s>0)$, C_1 (right broad solid line) by $k-k_1=se^{\pi i/2}$ $(s>0)$, C_2 (left dashed line) by $k=se^{7\pi i/6}$ $(\epsilon<s<\infty)$, C_3 (dashed arc) by $k=\epsilon e^{i\theta}$ $(-\pi/6<\theta<7\pi/6)$, and C_4 (right dashed line) by $k=se^{-\pi i/6}$ $(\epsilon<s<\infty)$ where ϵ is an infinitesimal constant.

$$I_-(n\pi r,t)=p^{1/2}\quad\text{for}\quad\frac{n\pi r}{t}>1. \quad (26)$$

Terms of exponentially small order with respect to t are omitted on the right-hand side of (26) (the same rule will be applied hereafter).

For $n\pi r/t<1$, on the other hand, contribution from the simple pole at $k=0$ vanishes because the path is raised over the range $-k_0<k<k_0$ as shown by a solid line in Fig. 2. Instead, we must estimate the integral in the vicinity of the stationary phase points $\pm k_0$ and the branch point $k_1\equiv ip/2r$ so that I_- is expressed by summation of these contributions

$$I_-(n\pi r,t)=I_-(n\pi r,t)|_{k=-k_0}+I_-(n\pi r,t)|_{k=k_0}+I_-(n\pi r,t)|_{k=k_1}\quad\text{for}\quad\frac{n\pi r}{t}<1. \quad (27)$$

The contribution to I_- from the stationary phase points $I_-|_{k=\pm k_0}$ is given by a straightforward application of the method shown in Lighthill,[21] and it becomes

$$I_-(n\pi r,t)|_{k=\pm k_0}=(\pm 2k_0r-ip)^{1/2}f(\pm k_0)\left(\frac{2\pi}{|\chi''_-(\pm k_0)|t}\right)^{1/2}\times\exp\left\{i\left[\chi_-(\pm k_0)t\mp\frac{\pi}{4}\right]\right\}+O(t^{-1}), \quad (28)$$

where

$$\chi''_-(k)\equiv\frac{d^2\chi_-}{dk^2}=-\frac{3n^2\pi^2k}{(k^2+n^2\pi^2)^{5/2}}. \quad (29)$$

The contribution to I_- from the branch point k_1 is obtained by evaluating the integral on the paths of integration C_0 $(k-k_1=se^{-3\pi i/2}$; s is real and positive) and C_1 $(k-k_1$

$=se^{\pi i/2}$) as shown by broad solid lines in Fig. 2. First, $\chi_-(k)$ is to be Taylor expanded about $k=k_1$ to give

$$\chi_-(k)=\chi_-(k_1)+\chi'_-(k_1)(k-k_1)+O(r^{-1}(k-k_1)^2,(k-k_1)^3), \tag{30}$$

where

$$\chi_-(k_1)=\frac{ip}{2}\left(\frac{1}{n\pi r}-\frac{1}{t}\right)+\frac{3\pi}{4t}+O(r^{-3}), \tag{31}$$

$$\chi'_-(k_1)=\frac{1}{n\pi}-\frac{r}{t}+O(r^{-2}). \tag{32}$$

Note that $\chi'_-(k_1)$ is real and positive for $n\pi r/t<1$ so that C_0 and C_1 correspond with paths of steepest decent. To avoid singularity at $k=0$, we first differentiate I_- with respect to t, and then estimate $\partial I_-/\partial t$ by Laplace's method[19] on these paths. Thus, we get, after integrating the obtained asymptotic solution of $\partial I_-/\partial t$ with respect to t,

$$I_-(n\pi r,t)|_{k=k_1}=\int_\infty^t\left[\frac{nr}{2(t'-n\pi r)^3}\right]^{1/2}\times\exp\left[-\frac{p}{2}\left(\frac{t'}{n\pi r}-1\right)\right]dt'+O(t^{-2}), \tag{33}$$

where (30)–(32) and $I_-|_{k=k_1}\to 0$ as $t\to\infty$ are used. Now we can get the solution of I_- for $n\pi r/t<1$ by substituting (28) and (33) into (27).

It should be noted, however, that the asymptotic behavior represented by (27) is not valid near $n\pi r/t=1$ where I_- has only one stationary point $k=k_0=0$ [see (25)]. According to Lighthill,[21] this region is called a caustic and the procedure to obtain the asymptotic behavior near the caustic is shown in his book. Now we try to apply his method to I_-. Noting that the integrand of I_- has a simple pole at $k=0$ [see (21) and (22)], we should deform the path of integration to C_2, C_3, and C_4 as shown by a dashed line in Fig. 2. Thus, we get

$$I_-(n\pi r,t)=\left(\int_{C_2}+\int_{C_3}+\int_{C_4}\right)\times(2kr-ip)^{1/2}\left[\frac{1}{2\pi k}+O(k)\right]\times\exp\left\{i\left[\chi_-(0)t+\chi'_-(0)tk+\frac{\chi^{(3)}_-(0)}{6}tk^3+O(tk^5)\right]\right\}dk, \tag{34}$$

where

$$\chi^{(3)}_-(0)\equiv\left.\frac{d^3\chi_-}{dk^3}\right|_{k=0}=-\frac{3}{n^3\pi^3}. \tag{35}$$

The function $(2kr-ip)^{1/2}$ on the right-hand side of (34) has a singularity at $k=k_1(=O(r^{-1}))$ so that a Taylor expansion of this function about $k=0$ is only valid for $|k|<O(r^{-1})$, which prevents us from properly evaluating (34) by the Airy integral. So I_- in (34) can only be reduced to a simplified form by the substitutions $k=[-2/\chi^{(3)}(0)t]^{1/3}e^{7\pi i/6}s$ and $k=[-2/\chi^{(3)}(0)t]^{1/3}e^{-\pi i/6}s$ for the first and the third integrals, respectively, which give

$$I_-(n\pi r,t)=\frac{2p^{1/2}}{3}+\int_0^\infty g(p,s)ds[1+O(t^{-2/3})]\quad\text{near}\quad\frac{n\pi r}{t}=1, \tag{36}$$

where

$$g(p,s)=\frac{i}{2\pi s}[h_+(p,s)-h_-(p,s)]\exp\left(-\frac{\alpha}{2}s-\frac{s^3}{3}\right), \tag{37}$$

and

$$h_\pm(p,s)=\left[2\left(\frac{2}{3t}\right)^{1/3}n\pi rs\exp\left(\pm\frac{\pi i}{3}\right)+p\right]^{1/2}\times\exp\left(\mp\frac{3^{1/2}}{2}\alpha si\right), \tag{38}$$

$$\alpha=\left(\frac{2}{3t}\right)^{1/3}(n\pi r-t). \tag{39}$$

Finally, substituting (26), (27), (36), and $I_+=0$ into (20), and carrying out the integration with respect to p, we obtain the asymptotic solution of I for large t:

$$I(n\pi r,t)=0\quad\text{for}\quad\frac{n\pi r}{t}>1, \tag{40}$$

$$I(n\pi r,t)=\frac{(n\pi r)^{4/3}}{3^{1/2}t^{1/3}k_0r}\sin[\omega_0(k_0)t-k_0r]+\frac{t}{[t^2-(n\pi r)^2]^{1/2}}+O(t^{-1})\quad\text{for}\quad\frac{n\pi r}{t}<1, \tag{41}$$

$$I(n\pi r,t)=\frac{1}{3}-\int_0^\infty p^{1/2}\exp(-p)dp\times\int_0^\infty g(p,s)ds[1+O(t^{-2/3})]\quad\text{near}\quad\frac{n\pi r}{t}=1, \tag{42}$$

where k_0 and $g(p,s)$ are given by (25) and (37), respectively. Note that we used

$$(\pm 2k_0r-ip)^{1/2}=(\pm 2k_0r)^{1/2}+O(r^{-1/2}) \tag{43}$$

in carrying out the integration with respect to p on the right-hand side of (20) when $n\pi r/t<1$. Equation (43) is valid except for $p>2k_0r\sim O(r)$ where the integrand on the right-hand side of (20) is exponentially small with respect to $r(\sim t)$.

The profiles of I at $t=100$ and 1000 are presented in Fig. 3. From this figure we see that the modal front propagates horizontally at the dimensionless long wave speed, $1/n\pi$. We also find that amplitude of I, which physically represents the velocity of the individual modes ($\sim r^{-1}I$) relative to the

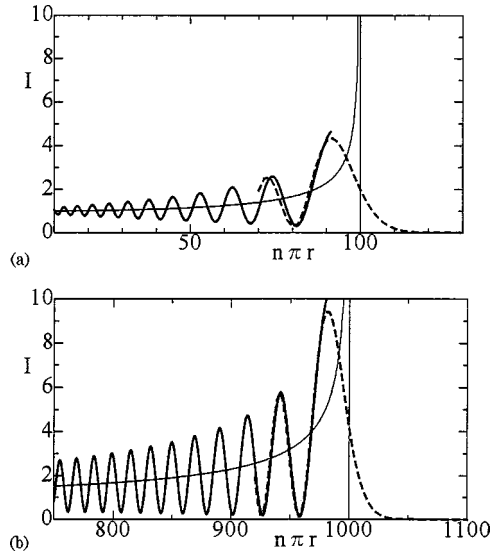

FIG. 3. The $n\pi r$ dependence of I: (a) $t=100$; (b) 1000. Broad solid lines show the results by solution (41) and broad dashed lines show the results by solution (42). Thin solid lines show the results by the solution under the hydrostatic approximation obtained by Lawrence (Ref. 15).

average flow velocity of the corresponding section ($\sim r^{-1}$), grows like $t^{1/3}$ at the modal front [see (38)], whereas for the two-dimensional modes it is $O(1)$ (see Kataoka *et al.*[7] and Mcewan and Baines[8]). The width of the front expands as $t^{1/3}$ [see (39)], which is the same order as that of the two-dimensional modes.[7,8] Behind the front, two types of waves are present. First, a long wave, that is generated continuously throughout the discharge, has radian frequency $\omega_0=0$ and horizontal wave number $k=0$. Second, the shorter waves, which are generated at the start of the discharge ($t=0$), have ω_0 and k both larger than zero. Both waves have the same order [$=O(1)$] in their amplitude of I [see the first and the second terms on the right-hand side of (41)]. If we compare with the case of the two-dimensional modes where the amplitude of the shorter waves decreases as $t^{-1/2}$ while that of the long wave is constant,[7,8] we can say that the shorter wave components are relatively dominant in the case of the cylindrical modes.

Also shown in Fig. 3 are profiles of the solution under the hydrostatic approximation obtained by Lawrence.[15] [There is an erratum in his solution (12). To obtain the correct form, $Nt/[(Nt)^2-(n\pi r/d)^2]^{1/2}$ should be multiplied by the second term on the right-hand side of his solution. See also Monismith *et al.*[22] where his solution is correctly reproduced.] This approximation is equivalent to ignoring vertical acceleration of fluids, or neglecting the first and second terms on the left-hand side of (12). The obtained solution is expressed by the combination of (40) and (41) with the first term on the right-hand side of (41) omitted. This solution represents the behavior of the long wave behind the modal front. However, it does not describe the shorter waves which have the same order of amplitude as that of the long wave.

IV. NUMERICAL METHOD

To investigate the point sink flow for arbitrary parameters, the system of equations (5)–(9) is solved numerically. The numerical method is the finite-difference method, and an extension of that used by Pao and Kao[4] for the two-dimensional line sink flow to the axisymmetric point sink flow. Some differences, however, exist between our method and theirs so that we make a brief explanation in the following especially focusing on these differences.

The time derivatives are approximated by the predictor–corrector method of second-order accuracy. The space derivatives are approximated by the central differences of second order except for the derivatives of ζ and ρ in the advective terms on the left-hand side of (5) and (6) where the usual upwind scheme of third-order accuracy (so-called UTOPIA) is used. The elliptic equation (7) is solved, subject to the boundary conditions (8), by the standard successive over relaxation technique to obtain the ψ field. The computational domain is $0<r<70$, $0<z<1$. The number of grids is 1200 (in the r direction)$\times$80 (in the z direction) for the flow in regime (i) ($\mathrm{Gr}=10^{10}$, $\mathrm{Sc}=730$; see also the first paragraph of Sec. V A) and 500×40 for the flow in regimes (ii) and (iii) (where all calculations are in the range $\mathrm{Gr}\leqslant10^6$). The grid points are concentrated toward the sink in the r direction to capture the motion of higher modes near the sink with higher accuracy. In the z direction, these are equally distributed. We apply the radiation condition[23] in terms of A representing one of the unknown variables ψ, ζ, and ρ:

$$\frac{\partial A}{\partial t}+C_r\frac{\partial A}{\partial r}=0 \tag{44}$$

at the upstream boundary $r=70$. Here we put $C_r=1/\pi$, or the long wave speed of the first mode. Calculations are continued even after the first mode arrives at this upstream boundary for the flow in regimes (ii) and (iii), so we need to evaluate the effects of this artificial open boundary. Indeed we have tested several cases where the open boundary is located much farther upstream and no detectable differences were found over the region $0<r<50$. For the flow in regime (i), however, calculations are terminated before the arrival of the first mode ($t=200$), since in this case $t=200$ is large enough to obtain the necessary information, such as the behavior of cylindrical modes and the steady-state withdrawal-layer thickness.

When calculating such an axisymmetric flow by the finite-difference method, we must note that the value of $w=-r^{-1}\partial\psi/\partial r$ cannot be properly evaluated at $r=0$. So the value of ρ cannot be obtained at $r=0$, since it is given by time integrating the evolution equation (6) which involves w. Therefore, in the present study, the vertical grid lines for ρ (and also ζ) are located to step over the axis of symmetry $r=0$ as shown in Fig. 4. These values are then obtained from the evolution equations (5) and (6) for $r>0$, and are determined on the added grids of $r<0$ from the boundary condition (8) as $\zeta(-\Delta r)=-\zeta(\Delta r)$ and $\rho(-\Delta r)=\rho(\Delta r)$ where Δr denotes the grid size on both sides of $r=0$ (see Fig. 4). Note that only ψ is defined at $r=0$ (see Fig. 4 again) where its value is directly given by (8).

To avoid singularity, we approximate the point sink by a small horizontal circular opening of finite radius r_w, and

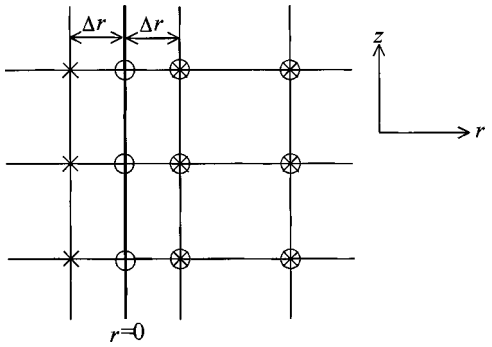

FIG. 4. A schematic of the computational grid near $r=0$ showing the definition points for ζ (×), ρ (×), and ψ (○).

introduce the following continuous function as a boundary condition for ψ:

$$\psi=\frac{2\pi^2}{r_w^2(\pi^2-4)}\int_{r_w}^{r} r'\left(1+\cos\frac{\pi r'}{r_w}\right)dr' \quad (0\leqslant r<r_w, z=0). \tag{45}$$

In fact, no physically appropriate boundary conditions for ζ and ρ can be found across this opening. Pao and Kao[4] applied $\zeta=0$ and $\rho=0$ in their numerical calculations of the line sink flow problem. It is clear, however, that neither ζ nor ρ keeps a constant value zero in the course of time, and these conditions lead to a distortion of their profiles near the opening. In the present study, ζ and ρ are assumed to be advected in the negative z direction. Thus, the boundary conditions for these variables are expressed by

$$\frac{\partial\zeta}{\partial t}+C_z\frac{\partial\zeta}{\partial z}=0,$$

$$\frac{\partial\rho}{\partial t}+C_z\frac{\partial\rho}{\partial z}=\frac{4\pi C_z}{F} \quad (0\leqslant r<r_w,\ z=0), \tag{46}$$

where $C_z=-(F/4\pi r)\partial\psi/\partial r$ and ψ is given by (45). Therefore the boundary condition (8) is replaced by (45) and (46) only on the boundary $0\leqslant r<r_w$, $z=0$. Throughout this paper r_w is set to be 0.15. We have also tested the smaller values of r_w and found no quantitative differences in the computational results except in the close vicinity of the sink.

V. NUMERICAL RESULTS

A. Cylindrical modes in an inviscid stratified fluid

The values of $\mathrm{Gr}=10^{10}$ and $\mathrm{Sc}=730$ were used to study the point sink flow of a stratified fluid where viscosity and diffusivity are negligible, because the flow for $\mathrm{Gr}=10^8$ was calculated to show that the effect of viscosity is too strong to investigate the essentially inviscid nature of flow patterns or the propagation of the individual modes. We have also tested the case of $\mathrm{Gr}=10^{12}$, and found that the behavior of the first and the second modes, including their amplitude and period of oscillation, is quantitatively almost unchanged at least until the maximum calculation time $t=200$. We have detected small differences in the amplitude of the mode $n\geqslant 3$ at large t, however, the difference is so small that we can say the Grashof number 10^{10} is large enough to know the fundamental mechanism of mode propagation in an inviscid stratified fluid. No quantitative differences were also detected in the flow of the Schmidt number larger than 730. Therefore, in Sec. V A and regime (i) of Sec. V B where inviscid, nondiffusive flow patterns are investigated, the parameters for Gr and Sc are set equal to 10^{10} and 730, respectively.

To see the behavior of the individual modes clearly, we define the strength of the nth mode as

$$u_n(x,t)=2r\int_0^1[u-u^{(\mathrm{pot})}]\cos n\pi z\,dz, \tag{47}$$

where $u^{(\mathrm{pot})}$ represents the velocity component in the r direction of a potential flow. The modal strength represents the ratio of the velocity component in the r direction of each mode at $z=0$ to the average flow speed ($=r^{-1}$) of the corresponding section. The obtained values of u_n ($n=1,2,3$) at $t=50$ and 100 are shown by broad lines in Fig. 5. Also shown by thin lines in the figures for $F=0.015$ are the values of u_n at $t=100$ calculated from the linear asymptotic solution ($F\to 0$) given by (40)–(42). Here the relation between u_n and I is obtained from (11), (15), and (16), as

$$u_n=-2I(n\pi r,t)-u_n^{(\mathrm{pot})}, \tag{48}$$

where $u_n^{(\mathrm{pot})}$ represents the strength of the nth mode by a potential flow, and is expressed by

$$u_n^{(\mathrm{pot})}=-2n\pi rK_1(n\pi r) \tag{49}$$

[see (14)]. Figure 5(a) shows that the first mode propagates upstream at nearly the linear long wave speed, $1/\pi$, whereas for the line sink flow it propagates at the speed $1/\pi-F_2$ (see Refs. 4–7 and 9). The difference in the propagation speed of wave modes between these two types of sinks is attributed to the fact that the average speed of the flow toward the sink decreases as r^{-1} in the case of point sink flow, but this velocity is constant ($=-F_2$) at any position in the case of line sink flow. We also find from Figs. 5(b) and 5(c) that the second and the third modes also propagate at the linear long wave speed, $1/2\pi$ and $1/3\pi$, respectively, although for large F, the modal front is located downstream side, since it is subject to the large-speed flow near the sink at the initial stage of propagation.

From these figures, it is seen that u_n for arbitrary F shows a relatively similar profile to that of $F\to 0$. In this regard, we have found that the strength of the modal front grows like $t^{1/3}$ for any value of F. However, the difference is seen in that, as F increases, the modal strength shows smoother profile, which indicates that the strength of the shorter waves is becoming smaller than that of the long wave. This is because the shorter waves have slower propagation speed and cannot propagate upstream at the initial stage when they are subject to the large-speed base flow toward the sink. The whole image of u_n also suggests that the absolute value of the modal strength is becoming smaller for a given n as F increases. Interpretation of this phenomenon is obtained by using the idea of a point of virtual control introduced by Ivey and Blake[18] (hereafter referred to as IB).

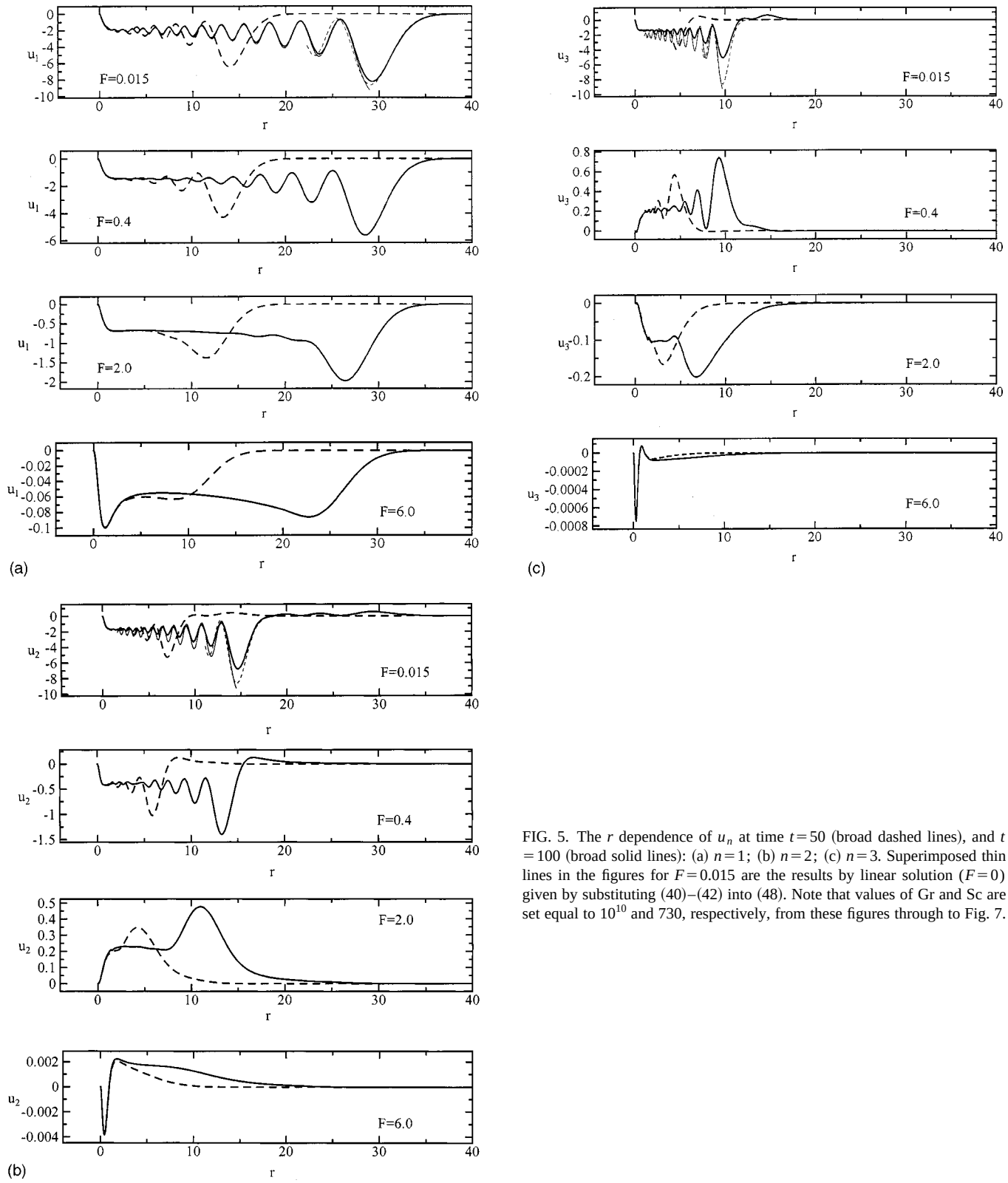

FIG. 5. The r dependence of u_n at time $t=50$ (broad dashed lines), and $t=100$ (broad solid lines): (a) $n=1$; (b) $n=2$; (c) $n=3$. Superimposed thin lines in the figures for $F=0.015$ are the results by linear solution ($F=0$) given by substituting (40)–(42) into (48). Note that values of Gr and Sc are set equal to 10^{10} and 730, respectively, from these figures through to Fig. 7.

They suggested that the flow patterns of regime (i) are determined by the upstream propagation of modes, and the behavior of these modes are influenced by the flow patterns at the point of virtual control. This point exists in the flow field where the local value of the internal Froude number F_i is unity. F_i is defined as the ratio of the average flow speed in a withdrawal layer to the propagation speed of mode whose vertical wavelength is equal to the withdrawal-layer thickness. In the present context, $F_i=F/4\delta^2 r$ where δ is half the dimensionless withdrawal-layer thickness, and this defines the location r_v of a point of virtual control as $r_v=F/4\delta^2$. IB experimentally observed that δ is $O(F^{1/3})$, which gives $r_v=O(F^{1/3})$. Consequently, each mode is influenced by the velocity distribution [here defined as $u_b(z)$] at

$r=r_v\sim F^{1/3}$. That is, $u_b(z)$ serves as the boundary condition on u of the upstream flow, and $u_b(z)$ can be decomposed into its modal components, each of which serves as a boundary condition for one mode of motion. As F, or equivalently r_v, increases, the profile of $ru_b(z)$ approaches that of uniform flow, since the withdrawal-layer thickness grows with r over the region $r<r_v$ where the advective effect overcomes the buoyancy effect. Accordingly, as F increases, the amplitude of each modal component of $r_v u_b(z)$ becomes smaller, and in effect, the modal strength [defined by (47)] for $r>r_v$ also becomes smaller.

Figure 5 also suggests that the modal strength becomes smaller as the modal number n increases for a given F. This fact can be explained by first considering the case of $F\to 0$ where $r_v u_b(z)$ is represented by the delta function. In this case, the same amount of modal strength is distributed to each mode. Therefore in the case of $F>0$, where $r_v u_b(z)$ exhibits smoother profile than that of $F\to 0$, the modal strength must decrease as n increases.

IB suggested that the higher modes, whose dimensionless vertical half-wavelength $\lambda(=1/n)$ is smaller than δ, cannot propagate upstream. Figure 5, however, shows that these higher modes ($n\geqslant 3$ for $F=0.4$, $n\geqslant 2$ for $F=2.0$ and 6.0) are propagating upstream despite the fact that $\lambda=1/n$ is smaller than δ [$\delta=0.52$, 0.88, and 1 for $F=0.4$, 2.0, and 6.0, respectively, which are obtained from (55)]. If we pay attention to the sign of each modal strength, it is seen that the strength of the lower modes with λ nearly equal to or larger than δ always has the same (negative) sign as that of the linear modes. On the other hand, the strength of the higher modes with λ smaller than δ does not necessarily have the same sign, but takes either sign. This means that the horizontal velocity at the intake level ($z=0$) of these higher modes is not always directed toward the sink. Therefore propagation of these higher modes does not contribute to net changes in the withdrawal-layer thickness. It is interesting to make a comparison with the case of line sink flow, in which the horizontal velocity at the intake level of the two-dimensional modes is always directed toward the sink.[7]

Last, we try to show that any mode can propagate upstream for any finite F by applying the idea of the point of virtual control to the case of large F where the fluid is withdrawn from all depths, that is, $\delta=1$. In this case a location of virtual control is $r_v=F/4$, which corresponds to the position where the propagation speed of the first mode and the average flow speed are identical. If we consider the case of $F\to\infty$ where the flow is potential and no stratification effects are present, the deviation from a uniform flow represented by (49) exists at any finite distance from the sink. Therefore it is natural to consider that the deviation also exists in the case of finite F where stratification effects are present. Thus, for finite F where r_v is finite, $u_b(z)$ is not uniform so that any mode can propagate upstream. This statement is consistent with the numerical results shown in Fig. 5 where any mode propagates upstream even for the large Froude number 6.0.

B. Steady-state withdrawal-layer thickness

IB introduced a scaling analysis to classify the steady-state flow patterns into the following three regimes. The dimensionless withdrawal-layer half-thickness δ and the dimensionless time to steady state in each regime are given as follows.

(i) Inertial-buoyancy regime (inertia and buoyancy forces are important):

$$\delta F^{-1/3}\sim 1 \quad \text{in} \quad t\sim t_s=F^{-1/3}r$$
$$[S>S_{\text{crit}},\quad r_c^{1/3}<O(1)]. \tag{50}$$

(ii) Viscous-convective regime (viscous forces and species convection are important):

$$\delta F^{-1/3}\sim S^{-1} \quad \text{in} \quad t\sim t_s=F^{-4/5}\,\text{Gr}^{-1/10}\,r^2$$
$$[S<S_{\text{crit}},\quad r_c^{1/3}<O(S^{-1})]. \tag{51}$$

(iii) Viscous-diffusive regime (viscous forces and species diffusion are important):

$$\delta F^{-1/3}\sim r_c^{1/3} \quad \text{in} \quad t\sim t_s=\text{Gr}^{1/6}\,\text{Sc}^{2/3}\,r^{2/3}$$
$$[S>S_{\text{crit}},\quad r_c^{1/3}>O(1)]$$

or

$$[S<S_{\text{crit}},\quad r_c^{1/3}>O(S^{-1})], \tag{52}$$

where

$$S=(F^4\,\text{Gr}^3)^{1/30}, \tag{53}$$

$$r_c=F^{-1}(\text{Gr}\,\text{Sc})^{-1/2}r. \tag{54}$$

IB obtained $S_{\text{crit}}\approx 3$ from their experiments and this value agrees well with our numerical results shown in the following [see (56)]. In this paper, we follow Imberger[10] by defining δ as the z coordinate at which u has dropped to 1/12 the value at $z=0$.

(i) Inertial-buoyancy regime. In Fig. 6, the time dependence of δ at $r=2$ and 4 for various values of F ($\text{Gr}=10^{10}$, $\text{Sc}=730$) is presented. The abscissa is dimensionless time scaled by $t_s=F^{-1/3}r$ [see (50)]. IB suggested that the time to steady state is $t\approx 4t_s$, and Spigel and Farrant[17] suggested $t\approx 2.5t_s$ from their experiments. These experimental results are only for the flow of $F<0.04$ and we see a good agreement with our numerical results for small F (see the results for $F=0.002$ and 0.015 in Fig. 6). Figure 6, however, suggests that the scaled time t/t_s to steady state is not constant with respect to F and takes larger value as F increases.

In Fig. 7, the steady-state value of δ is shown as a function of $F^{1/3}$. Figure 7 suggests that

$$\delta F^{-1/3}=0.70 \tag{55}$$

is a good description of the results, and it agrees well with the experimental results: $\delta F^{-1/3}=0.66$ by IB; $\delta F^{-1/3}=0.81$ by Spiegel and Farrant;[17] and $\delta F^{-1/3}=0.70$ by Lawrence.[15] As mentioned previously, however, their experiments were only concerned with the flow of $F<0.04$. Therefore the importance of our result is that formula (55) is valid even for

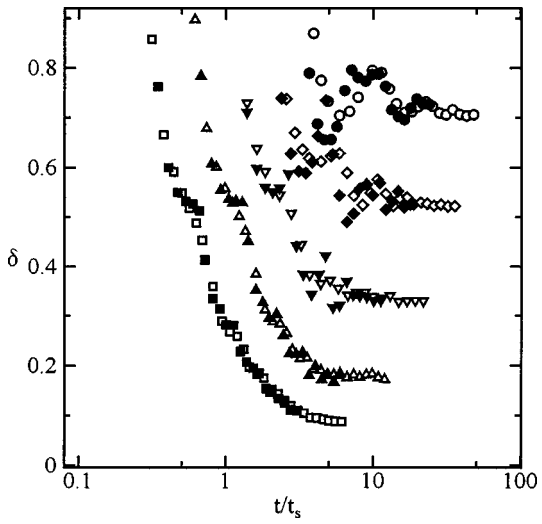

FIG. 6. Time development of dimensionless withdrawal-layer half-thickness δ for the inertial-buoyancy regime: □, ■, $F=0.002$; △, ▲, 0.015; ▽, ▼, 0.1; ◇, ◆, 0.4; ○, ●, 1.0. Open and closed marks represent results at $r=2$ and 4, respectively.

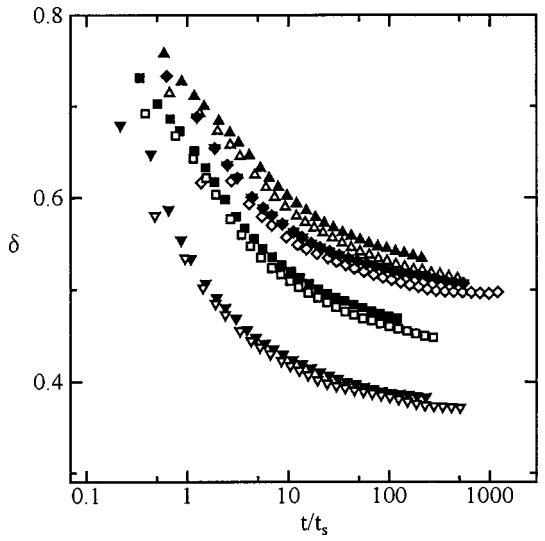

FIG. 8. Time development of dimensionless withdrawal-layer half-thickness δ for the viscous-convective regime (Sc=∞): ▽, ▼, $(F,\mathrm{Gr})=(0.04,10^4)$; □, ■, $(0.04,10^3)$; ◇, ◆, $(0.15,10^4)$; △, ▲, $(0.08,10^3)$. Open and closed marks represent results at $r=2$ and 3, respectively.

large F where δ approaches the value 1. This fact indicates that the steady-state withdrawal-layer thickness of regime (i) is not influenced by the presence of the upper plane.

From all the above-mentioned arguments about the inviscid stratified flow including those in Sec. V A, we can say that the critical Froude number F_c of the point sink flow depends on its definition. If it is the Froude number defined to demarcate whether or not the selective withdrawal occurs ($\delta<1$ or not), we obtain $F_c=2.9$ from (55). If it is defined to distinguish whether internal wave modes can propagate upstream or not, we obtain $F_c=\infty$ from the discussion in the last paragraph of Sec. V A. In the case of line sink flow, both values are identical with $F_{2c}=1/\pi$ (see Refs. 2 and 11).

(ii) Viscous-convective regime. To clarify only the viscous effects of fluid and the corresponding flow patterns, the parameter Sc of numerical results in regime (ii) is set to be infinity. According to the scaling analysis,[18] the withdrawal-layer thickness in this regime is independent of distance from the sink [see (51)]. Therefore, as time increases, any mode is expected to reach far upstream with its strength approaching some constant steady-state value independent of r. Indeed this phenomenon was also observed in our numerical results, but the time to steady state was extremely longer than was suggested by prior works.

Figure 8 shows the time dependence of δ for the flow of this regime. The abscissa is the dimensionless time scaled by $t_s=F^{-4/5}\mathrm{Gr}^{-1/10}r^2$ [see (51)]. Figure 8 suggests that the time to steady state is about $t\approx 500t_s$, which is totally different from the experimental result $t\approx 3t_s$ suggested by IB. One of the possible reasons for this discrepancy is the geometrical difference that the experiment is conducted in a bounded container while the numerical results are for a horizontally unbounded fluid. We can also point out the difficulty in defining the withdrawal-layer thickness in their experiments, since the induced velocity is small in the point sink flow. Anyway, our numerical results suggest that the time to steady state is very long in an infinite-horizontal-extent fluid which is often encountered in practical situations, such as oceans, lakes, and large reservoirs.

It is time consuming to calculate until $t=500t_s$ for various sets of parameters. Therefore, in Fig. 9, we have plotted δ at $t=300t_s$ where δ is considered to reach nearly the steady-state value. Also shown in Fig. 9 is the steady-state value of δ in regime (i). The ordinate is $\delta F^{-1/3}$ and the abscissa is S^{-1}. Figure 9 suggests that

$$\delta F^{-1/3}=1.3S^{-1}+0.2 \quad \text{for } S<S_{\mathrm{crit}}=3 \tag{56}$$

is a good description of the results of regime (ii), and it estimates the value of δ moderately smaller than the experimental results $\delta F^{-1/3}=2.1S^{-1}$ of IB. However, this discrepancy is consistent if we note again the geometrical differ-

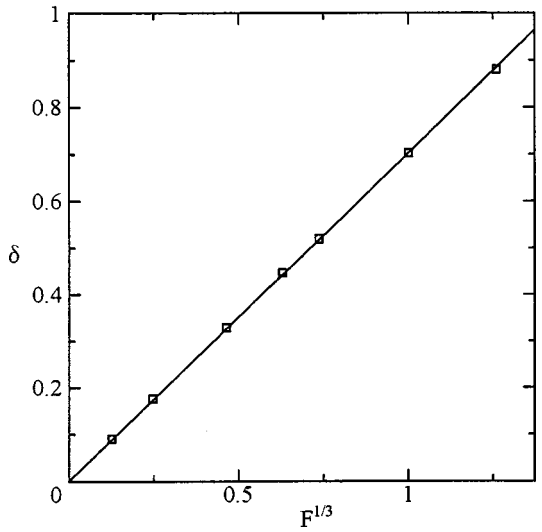

FIG. 7. Steady-state withdrawal-layer half-thickness δ as a function of $F^{1/3}$ for the inertial-buoyancy regime. The symbols represent the numerical results and the solid line is a fit to these numerical data.

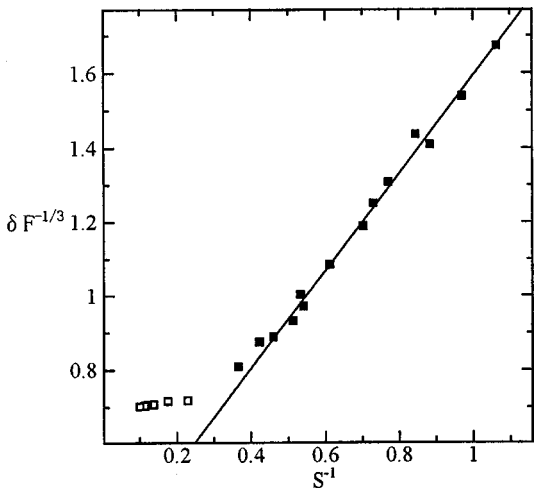

FIG. 9. Steady-state value of $\delta F^{-1/3}$ as a function of S^{-1}. □: The results for the inertial-buoyancy regime whose parameters are in the range $0.002 \leqslant F \leqslant 1.0$ with $\mathrm{Gr}=10^{10}$ and $\mathrm{Sc}=730$. ■: The results for the viscous-convective regime whose parameters are in the range $0.01 \leqslant F \leqslant 0.2$ and $10^2 \leqslant \mathrm{Gr} \leqslant 10^6$ with $\mathrm{Sc}=\infty$. The solid line is a fit to the data for the viscous-convective regime.

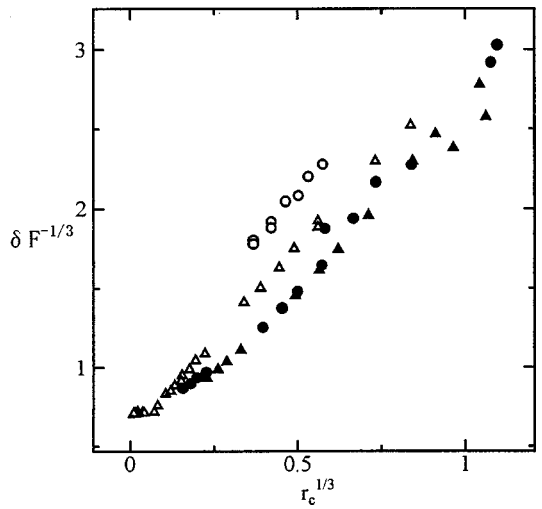

FIG. 10. Steady-state value of $\delta F^{-1/3}$ as a function of $r_c^{1/3}$: ▲, Sc=7; ●, 64; △, 730; ○, 10 000. The other parameters are in the range $0.001 \leqslant F \leqslant 0.2$ and $10^2 \leqslant \mathrm{Gr} \leqslant 10^{10}$.

ence, and also that δ in our case is defined as the z coordinate at which u has dropped to 1/12, whereas for their experiments it is defined as the vertical coordinate z at which the horizontal velocity first becomes zero.

(iii) Viscous-diffusive regime. In this regime we have found that δ approaches its steady-state value in time $t \approx 2t_s$ where t_s is given by (52). Taking the time to steady state as $t=2t_s$, we have plotted the steady-state values of δ in Fig. 10. The ordinate is $\delta F^{-1/3}$ and the abscissa is $r_c^{1/3}$ whose definition is given by (54). From Fig. 10 we see that in regime (iii), where $r_c^{1/3} \gtrsim 0.3$, $\delta F^{-1/3}$ is dependent not only on r_c but also on Sc so that the withdrawal-layer thickness is expressed by

$$\delta F^{-1/3} = 2.4 r_c^{1/3} + h(\mathrm{Sc}), \tag{57}$$

where $h(\mathrm{Sc})$ is a monotonically increasing function of Sc. This formula is in relatively good agreement with Koh's analytical result[16] $\delta F^{-1/3} = 2.9 r_c^{1/3}$ except for the dependence on Sc. Such a dependence on Sc was also found in the case of line sink flow.[10]

Here we should mention that formula (57) is not always valid when δ approaches the value 1, and all the plotted data in Fig. 10 are those for $\delta < 0.5$. Some data for $\delta > 0.5$ deviate from this formula due to the influence of the upper plane. If we recall that δ in regime (i) is not influenced by this effect, we are now tempted to consider the mechanism why δ in regime (iii) is influenced by the presence of the upper plane while that in regime (i) is not. This explanation can be given in the following manner by considering the propagation of modes. In regime (i) all modes can propagate upstream so that summation of velocity profiles of all modes can describe arbitrary horizontal velocity distribution. In regime (iii), however, we have found that the higher modes cannot propagate far upstream due to species diffusion, that is, the number of modes that are present at any distance from the sink is finite. Therefore, description of arbitrary velocity profiles is impossible and δ is substantially influenced by the mode shape which is dependent on the depth of the fluid. From this argument it is expected that δ in regime (ii) is not influenced by this effect at the steady state, since all modes can propagate far upstream.

VI. CONCLUDING REMARKS

We have studied the point sink flow of linearly stratified fluid in an infinite-horizontal-extent domain of finite depth. We summarize the main results into the following three parts.

First, we have considered the case of $F \to 0$, $\mathrm{Gr} \to \infty$, and $\mathrm{Gr}^{1/2}\,\mathrm{Sc} \to \infty$ to obtain a linear asymptotic solution for large t of the cylindrical modes in a stratified fluid where viscous and diffusive effects are negligible. The obtained solution is subject to no wavelength approximation and represents the wave nature clearly. It is found that the amplitude of the modal strength grows like $t^{1/3}$ at the front, unlike its two-dimensional counterpart, which is $O(1)$. Behind the front two types of waves with the long and the shorter horizontal wavelength are present. Both waves have their amplitude of $O(1)$ which indicates that the shorter waves are relatively dominant compared to the case of the two-dimensional modes.

Second, we have numerically studied the mode propagation for $F>0$ in an essentially inviscid stratified fluid ($\mathrm{Gr}=10^{10}$). It is seen that the modal strength generally becomes smaller as F increases, and for constant value of F, as the modal number increases. The strength of the higher modes can take an opposite sign to that of the linear modes. We also suggested that any mode can propagate far upstream for any finite F.

Finally, we have examined the withdrawal-layer thickness for all three regimes suggested by IB. In the inertial-buoyancy regime the thickness is not influenced by the presence of the upper plane and the selective withdrawal ceases to occur at $F=2.9$. In the viscous-convective regime an ex-

tremely long time is necessary to establish the steady state and the withdrawal-layer thickness is moderately smaller than the prior experimental results. In the viscous-diffusive regime the dependence of the withdrawal-layer thickness on Sc is newly found. Only in this last regime could the thickness be influenced by the presence of the upper plane.

We conclude this study by briefly mentioning the effect of rotation. Whitehead[24] found experimentally that such a rotation has the effect of thickening the withdrawal layer. Monismith *et al.*[22] suggested the same effect by scaling argument. The latter authors also investigated the behavior of linear cylindrical modes in an inviscid stratified fluid under the hydrostatic approximation. We are now currently investigating the propagation of these cylindrical modes on the basis of the full linear equations, and studying the flow patterns under rotation over the entire parameter range numerically. These matters will be reported elsewhere.

[1]J. Imberger and J. C. Patterson, ''Physical limnology,'' Adv. Appl. Mech. **27**, 303 (1990).
[2]C.-S. Yih, ''On the flow of a stratified fluid,'' *Proceedings of the Third U.S. National Congress on Applied Mechanics* (ASME, New York, 1958), pp. 857–861.
[3]W. R. Debler, ''Stratified flow into a line sink,'' J. Eng. Mech. Div., Am. Soc. Civ. Eng. **85**, 51 (1959).
[4]H.-P. Pao and T. W. Kao, ''Dynamics of establishment of selective withdrawal of a stratified fluid from a line sink. 1. Theory,'' J. Fluid Mech. **65**, 657 (1974).
[5]T. W. Kao, H.-P. Pao, and S. N. Wei, ''Dynamics of establishment of selective withdrawal of a stratified fluid from a line sink. 2. Experiment,'' J. Fluid Mech. **65**, 689 (1974).
[6]S. R. Clarke and J. Imberger, ''The effect of shear in selective withdrawal,'' Phys. Fluids **7**, 1523 (1995).
[7]T. Kataoka, M. Tsutahara, and S. Mizutani, ''Selective withdrawal through a line sink of non-rotating and rotating stratified fluid in a reservoir of finite depth,'' Eur. J. Mech. B/Fluids (to be published).
[8]A. D. Mcewan and P. G. Baines, ''Shear fronts and an experimental stratified shear flow,'' J. Fluid Mech. **63**, 257 (1974).
[9]J. Imberger, R. Thompson, and C. Fandry, ''Selective withdrawal from a finite rectangular tank,'' J. Fluid Mech. **78**, 489 (1976).
[10]J. Imberger, ''Two-dimensional sink flow of a stratified fluid contained in a duct,'' J. Fluid Mech. **53**, 329 (1972).
[11]C.-S. Yih, *Stratified Flows* (Academic, New York, 1980), pp. 110–122.
[12]M. S. Ingber and A. K. Mitra, ''Numerical solution of stratified flow into a sink: A criterion for selective withdrawal,'' J. Fluids Eng. **109**, 384 (1987).
[13]C.-S. Yih and S. Zhu, ''Selective withdrawal from stratified streams,'' J. Aust. Math. Soc. B, Appl. Math. **38**, 26 (1996).
[14]C.-S. Yih, ''On the nonexistence of solution of a differential system governing axisymmetric flow of a stratified fluid,'' Q. Appl. Math. (April 1982), p. 101.
[15]A. Lawrence, ''Selective withdrawal through a point sink,'' Proceedings of the Second International Symposium on Stratified Flows, Tapir, 1980 (unpublished), pp. 411–425.
[16]R. C. Y. Koh, ''Viscous stratified flow toward a sink,'' J. Fluid Mech. **24**, 555 (1966).
[17]R. H. Spiegel and B. Farrant, ''Selective withdrawal through a point sink and pycnocline formation in a linearly stratified flow,'' J. Hydraul. Res. **22**, 35 (1984).
[18]G. N. Ivey and S. Blake, ''Axisymmetric withdrawal and inflow in a density-stratified container,'' J. Fluid Mech. **161**, 115 (1985) (referred to herein as IB).
[19]C. M. Bender and S. A. Orszag, *Advanced Mathematical Methods for Scientists and Engineers* (McGraw–Hill, New York, 1978), Chap. 6.
[20]S. Moriguchi, K. Udagawa, and S. Hitotsumatsu, *Mathematical Formulae* (Iwanami, Tokyo, 1960), p. 179 (in Japanese).
[21]J. Lighthill, *Waves in Fluids* (Cambridge University Press, Cambridge, 1978), Secs. 3.7 and 4.11.
[22]S. G. Monismith, N. R. Mcdonald, and J. Imberger, ''Axisymmetric selective withdrawal in a rotating stratified fluid,'' J. Fluid Mech. **249**, 287 (1993).
[23]R. A. Pearson, ''Consistent boundary conditions for numerical models of systems that admit dispersive waves,'' J. Atmos. Sci. **31**, 1481 (1974).
[24]J. A. Whitehead, ''Selective withdrawal of a rotating stratified fluid,'' Dyn. Atmos. Oceans **5**, 123 (1980).